Bose–Einstein condensation of semi-hard bosons in the $S = 1$ dimerized organic compound F_2PNNNO

2010 J. Phys.: Condens. Matter 22 036001

(http://iopscience.iop.org/0953-8984/22/3/036001)

J. Phys.: Condens. Matter **22** (2010) 036001 (9pp) doi:10.1088/0953-8984/22/3/036001

Bose–Einstein condensation of semi-hard bosons in the $S = 1$ dimerized organic compound F_2PNNNO

I G Bostrem[1], V E Sinitsyn[1], A S Ovchinnikov[1], Y Hosokoshi[2] and K Inoue[3]

[1] Department of Physics, Ural State University, 620083, Ekaterinburg, Russia
[2] Department of Physical Science, Osaka Prefecture University, Osaka, Japan
[3] Department of Chemistry, Hiroshima University, Hiroshima, Japan

Received 24 August 2009, in final form 28 October 2009
Published 16 December 2009
Online at stacks.iop.org/JPhysCM/22/036001

Abstract
An analysis of the energy spectrum and magnetization curve of the two-dimensional organic antiferromagnet F_2PNNNO with a spin-one dimerized structure shows that the behavior of the compound in an external magnetic field can be explained within a lattice boson model with an extended Pauli exclusion principle, i.e. no more than two bosons per dimer. The unusual magnetization curve observed experimentally in the compound reflects a sequence of phase transitions intrinsic for a lattice boson system with strong on-site and inter-site repulsions due to a tuning of magnon density by the applied magnetic field.

1. Introduction

The possibility of studying Bose–Einstein condensation (BEC) with low-dimensional magnetic materials predicted theoretically twenty years ago [1] gave rise to intense experimental research in the field. The analogy between the spins and the bosons becomes evident for antiferromagnets where spins form dimers with a spin-singlet ground state [2]. Originally, the attention was mainly focused on spin-1/2 systems where excitations inside each dimer (triplons) were regarded as bosons with hard-core repulsion, i.e. no more than one boson was presented on a single dimer. The analogy enables the treatment of spin systems as interacting bosons whose ground state is determined by the balance between kinetic energy and repulsive interactions [3]. If the repulsion dominates, the bosons form a superlattice and a finite energy cost is needed to create an additional particle. This is exhibited as a jump in the chemical potential versus boson number, in spin language, as a plateau in the magnetization curve versus magnetic field at a rational fraction of the saturated magnetization.

The field induced condensation of magnons has been experimentally observed in coupled quantum ($s = 1/2$) dimer systems based on Cu^{2+} ions such as $TlCuCl_3$, $BaCuSi_2O_6$ [4–6] and the compound $Ba_2Cr_2O_8$ [7] which are adequately described by the BEC theory.

Recently, the magnetic weakly coupled dimer system $Ba_3Mn_2O_8$ with $S = 1$ moments has attracted a lot of attention [8, 9]. The field behavior of magnetization in the system of antiferromagnetically weakly coupled $S = 1$ dimers can be described as BEC of magnons by mapping the spin-1 system into a gas of semi-hard-core bosons [10]. Considering the example of a simple two-dimensional (2D) $S = 1$ isotropic Heisenberg model with a dimerized structure and frustrating interactions, it was suggested that an emergence of the spin supersolid state (a long-range mixing of superfluid and charge-ordered phases) was induced by a magnetic field [11]. The organic compound F_2PNNNO is another example of a spin-one dimer based magnetic insulator. This is a 2D Heisenberg system with a singlet ground state, in which $S = 1$ dimers interact antiferromagnetically [12, 13]. The lattice of the system is equivalent to the honeycomb one (figure 1). The field magnetization process shows a two-step saturation behavior that is a rare example of observing a plateau in a two-dimensional system. The intermediate plateau corresponds to the half value of saturation magnetization. The consistent calculation of susceptibility and magnetization for the finite-size cluster with imposed periodic conditions yields the following estimations of antiferromagnetic exchange couplings, $2J_0 = 67.5$ K, $2J_1 = 7.5$ K, i.e. the system can be regarded as a real 2D dimerized spin-one system.

Apparently, the quantum antiferromagnet F_2PNNNO offers an opportunity to verify the relevance of the semi-

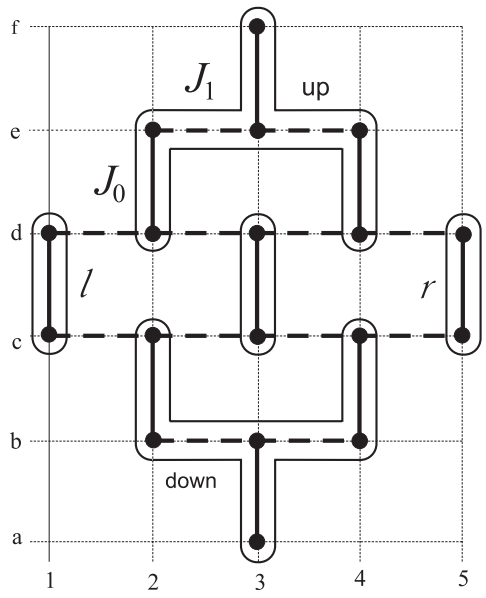

Figure 1. The 18-site cluster used in numerical calculations. The environment of the central dimer consists of two 'fork'-like parts (up and down), and the left (l) and the right (r) dimers. The intra-dimer J_0 and the inter-dimer J_1 interactions are shown by solid and dotted lines, respectively.

hard-core boson model for the description of a dimerized system. In this paper, we perform diagonalization of the finite cluster of $N = 18$ sites, calculate the magnetization and demonstrate that these results can be easily understood within the semi-hard boson model with strong on-site and inter-site repulsions. The diagonalization procedure we used exploits the spin rotational symmetry [14, 15]. The implementation of non-Abelian $SU(2)$ spin symmetry is based on an elimination of quantum numbers via the Wigner–Eckart theorem. The advantage of the approach is that the cluster spin states are decomposed into different sectors of the total cluster spin. In addition, one can independently handle each of the target spin states.

The paper is organized as follows. The model and the diagonalization algorithm are given in section 2. The truncation procedure is discussed in section 3. In section 4 we report numerical cluster calculations of the spectrum and the magnetization curve. The analogy with the lattice boson model is performed in section 5. The main results are recapitulated in the conclusion.

2. The model

The Hamiltonian of weakly interacting spin-one dimers on the 2D lattice depicted in figure 1 is given by

$$H_S = J_0 \sum_i \vec{S}_{i1}\vec{S}_{i2} + J_1 \sum_{\langle i\alpha, j\bar{\alpha}\rangle} \vec{S}_{i\alpha}\vec{S}_{j\bar{\alpha}}, \qquad (1)$$

where J_0 is the coupling inside the ith dimer, J_1 is the strength of the exchange interaction between the dimers located on the bonds $\langle i, j\rangle$. The indices $\alpha, \bar{\alpha}$ mark $S = 1$ spins that enter into the interacting dimers, namely, $\bar{\alpha} = 1, 2$ provided $\alpha = 2, 1$, respectively. Both types of interactions are antiferromagnetic $J_{0,1} > 0$, and the regime of weakly interacting dimers, $|J_0| \gg |J_1|$, is considered. The Heisenberg model has been previously suggested to explain some thermodynamical properties of F_2PNNNO [12]. Numerical calculations based on the Hamiltonian (1) via exact diagonalization of small clusters and their comparison with experimental data prove its relevance for the ratio $|J_1/J_0| \ll 1$. The dimerization caused by the anisotropy of interactions on a lattice is somewhat analogous to the situation in two-leg spin-1 antiferromagnetic ladders in a strong antiferromagnetic rung-coupling regime, when the ladder ground state is well approximated by the tensor product of singlet rung-dimers [16].

To get the energy spectrum, finite-size clusters composed of $N = 10$ and 18 sites are selected. In a choice of the cluster, care should be taken to ensure that the lattice point group symmetry holds. Since intra-dimer interactions are the strongest, the cluster should contain whole dimers and not break them into parts. To mark sites inside the cluster, chessboard-like notations will be used, where site positions along the x axis are marked by numbers whereas positions along the y axis are denoted by Latin letters.

To find eigenfunctions of the cluster that inherit the total cluster spin as a quantum number, we should develop a consecutive procedure for adding spin moments. It is convenient to break the cluster into several parts. Following the strategy of building a cluster used in [15], one should identify the central dimer (center) and its environment. The center is composed of $c3$ and $d3$ sites whereas other sites are embodied into the environment.

The Hamiltonian of the central dimer has the form $H_c = J_0\vec{S}_{c3}\vec{S}_{d3}$, whereas the interaction between the center and its environment is given by

$$V_{ce} = J_1\vec{S}_{c3}(\vec{S}_{c2} + \vec{S}_{c4}) + J_1\vec{S}_{d3}(\vec{S}_{d2} + \vec{S}_{d4}). \qquad (2)$$

The environment consists of four parts, namely of two dimers, left (l) and right (r) ones, with the Hamiltonians

$$H_l = J_0\vec{S}_{c1}\vec{S}_{d1}, \qquad \text{and} \qquad H_r = J_0\vec{S}_{c5}\vec{S}_{d5}, \qquad (3)$$

respectively, as well as two fork-like parts, i.e. the down and up ones, with the corresponding Hamiltonians

$$H_{down} = J_0(\vec{S}_{b2}\vec{S}_{c2} + \vec{S}_{a3}\vec{S}_{b3} + \vec{S}_{b4}\vec{S}_{c4}) + J_1\vec{S}_{b3}(\vec{S}_{b2} + \vec{S}_{b4}), \quad (4)$$

$$H_{up} = J_0(\vec{S}_{d2}\vec{S}_{e2} + \vec{S}_{e3}\vec{S}_{f3} + \vec{S}_{d4}\vec{S}_{e4}) + J_1\vec{S}_{e3}(\vec{S}_{e2} + \vec{S}_{e4}). \quad (5)$$

The interaction between the left/right dimers and the fork-like parts is presented as

$$V_{env} = J_1(\vec{S}_{c2}\vec{S}_{c1} + \vec{S}_{d2}\vec{S}_{d1} + \vec{S}_{c4}\vec{S}_{c5} + \vec{S}_{d4}\vec{S}_{d5}). \qquad (6)$$

The Hamiltonian of the entire cluster gathers all the above terms

$$H = H_c + V_{ce} + \{H_l + H_r + H_{down} + H_{up} + V_{env}\}. \qquad (7)$$

There are three states of dimer, an elementary block of the cluster, with total spin $S_{dm} = 0$ (singlet), $S_{dm} = 1$ (triplet), and $S_{dm} = 2$ (quintuplet). The energies of the states are

$E_0 = -2J_0$, $E_1 = -J_0$, $E_2 = J_0$, respectively, and the eigenstates are obtained via the common rule of the addition of moments

$$|11; S_{\rm dm}M_{\rm dm}\rangle \equiv |S_{\rm dm}M_{\rm dm}\rangle = \sum_{\sigma_1\sigma_2}\begin{bmatrix} 1 & 1 & S_{\rm dm} \\ \sigma_1 & \sigma_2 & M_{\rm dm}\end{bmatrix}|1\sigma_1\rangle|1\sigma_2\rangle, \tag{8}$$

where $[\cdots]$ is the Clebsch–Gordan coefficient. To increase the size of cluster, reduced matrix elements (RME) of the operators $S(1)$ and $S(2)$, that constitute the dimer, calculated within the basis (8), are needed

$$\langle S_{\rm dm}\|S(1)\|S'_{\rm dm}\rangle = (-1)^{1+S'_{\rm dm}}\sqrt{(2S_{\rm dm}+1)(2S'_{\rm dm}+1)} \times \begin{Bmatrix} S_{\rm dm} & 1 & S'_{\rm dm} \\ 1 & 1 & 1\end{Bmatrix}\langle 1\|S\|1\rangle, \tag{9}$$

$$\langle S_{\rm dm}\|S(2)\|S'_{\rm dm}\rangle = (-1)^{1+S_{\rm dm}}\sqrt{(2S_{\rm dm}+1)(2S'_{\rm dm}+1)} \times \begin{Bmatrix} S_{\rm dm} & 1 & S'_{\rm dm} \\ 1 & 1 & 1\end{Bmatrix}\langle 1\|S\|1\rangle, \tag{10}$$

where $\{\cdots\}$ is the $6j$-symbol of the rotational group, and the reduced matrix element $\langle 1\|S\|1\rangle = \sqrt{6}$.

The fork-like part includes three interacting dimers. It is convenient to build the basis of this fragment according to the scheme $(2+4)+3$ of moment addition, i.e. combining the 'prong' dimer functions is followed by adding the 'handle' function. As a result, the basic functions with total spin $S_{\rm down}$ of the down fork-like part have the form

$$|(S_2S_4)S_{24}, S_3; S_{\rm down}M_{\rm down}\rangle = \sum_{M_2M_3M_4M_{24}}\begin{bmatrix} S_2 & S_4 & S_{24} \\ M_2 & M_4 & M_{24}\end{bmatrix} \times \begin{bmatrix} S_{24} & S_3 & S_{\rm down} \\ M_{24} & M_3 & M_{\rm down}\end{bmatrix}|S_2M_2\rangle|S_3M_3\rangle|S_4M_4\rangle, \tag{11}$$

where S_2, S_3 and S_4 are the spins of dimers composed of the $b2$ and $c2$ sites, etc. Within the basis, the Hamiltonian (4) is presented by the block diagonal 141×141 matrix. The blocks are marked by total spin $S_{\rm down} = 0, 1, \ldots, 6$ values. A diagonalization of the $H_{\rm down}$ matrix yields the spectrum $E_{i_{\rm down}S_{\rm down}}$ and eigenfunctions

$$|i_{\rm down}S_{\rm down}M_{\rm down}\rangle = \sum_{S_2S_3S_4S_{24}}\alpha^{i_{\rm down}S_{\rm down}}_{(S_2S_4)S_{24},S_3}|(S_2S_4)S_{24}, S_3; S_{\rm down}M_{\rm down}\rangle,$$

where the $i_{\rm down}$ index distinguishes basic functions with the same total $S_{\rm down}$ spin. The results for the upper fork-like part can be obtained the same way provided the site $c4$ is substituted for $d2$, and $c2$ is changed for $d4$ etc. The assembly of the cluster part is completed by calculations of the reduced matrix elements (see equation (A.1) in appendix A).

In the next step, we construct spin functions of the non-interacting parts, i.e. of the left and of the right dimers

$$|S_{\rm l}S_{\rm r}; S_{\rm lr}M_{\rm lr}\rangle = \sum_{M_{\rm l}M_{\rm r}}\begin{bmatrix} S_{\rm l} & S_{\rm r} & S_{\rm lr} \\ M_{\rm l} & M_{\rm r} & M_{\rm lr}\end{bmatrix}|S_{\rm l}M_{\rm l}\rangle|S_{\rm r}M_{\rm r}\rangle, \tag{12}$$

where $S_{\rm lr} = 0, 1\ldots, 4$, and upper and lower fork-like parts

$$|i_{\rm up}S_{\rm up}i_{\rm down}S_{\rm down}; S_{\rm ud}M_{\rm ud}\rangle = \sum_{M_{\rm up}M_{\rm down}}\begin{bmatrix} S_{\rm up} & S_{\rm down} & S_{\rm ud} \\ M_{\rm up} & M_{\rm down} & M_{\rm ud}\end{bmatrix} \times |i_{\rm up}S_{\rm up}M_{\rm up}\rangle|i_{\rm down}S_{\rm down}M_{\rm down}\rangle, \tag{13}$$

where $S_{\rm ud} = 0, 1\ldots, 12$, and add them together to build the basis of environment for the central dimer

$$|(i_{\rm up}S_{\rm up}i_{\rm down}S_{\rm down})S_{\rm ud}, (S_{\rm l}S_{\rm r})S_{\rm lr}; S_{\rm env}M_{\rm env}\rangle = \sum_{M_{\rm ud}M_{\rm lr}}\begin{bmatrix} S_{\rm ud} & S_{\rm lr} & S_{\rm env} \\ M_{\rm ud} & M_{\rm lr} & M_{\rm env}\end{bmatrix}|i_{\rm up}S_{\rm up}i_{\rm down}S_{\rm down}; S_{\rm ud}M_{\rm ud}\rangle \times |S_{\rm l}S_{\rm r}; S_{\rm lr}M_{\rm lr}\rangle. \tag{14}$$

The reduced matrix elements of spin operators required to build the Hamiltonian of the environment are shown in appendix A (see equations (A.2)–(A.5)). Note, that the number of states (14) is too great to avoid the truncation procedure (see section 3).

The matrix elements of the environment Hamiltonian $H_{\rm env} = H_{\rm l} + H_{\rm r} + H_{\rm down} + H_{\rm up} + V_{\rm env}$ are listed below

$$\begin{aligned}
&\langle (i_{\rm up}S_{\rm up}i_{\rm down}S_{\rm down})S_{\rm ud}, (S_{\rm l}S_{\rm r})S_{\rm lr}; S_{\rm env}M_{\rm env}|H_{\rm env} \\
&\quad\times |(i'_{\rm up}S'_{\rm up}i'_{\rm down}S'_{\rm down})S'_{\rm ud}, (S'_{\rm l}S'_{\rm r})S'_{\rm lr}; S'_{\rm env}M'_{\rm env}\rangle \\
&= (E_{i_{\rm up}S_{\rm up}} + E_{i_{\rm down}S_{\rm down}} + E_{S_{\rm l}} + E_{S_{\rm r}})\delta_{i_{\rm up},i'_{\rm up}}\delta_{S_{\rm up},S'_{\rm up}}\delta_{i_{\rm down},i'_{\rm down}} \\
&\quad\times \delta_{S_{\rm down},S'_{\rm down}}\delta_{S_{\rm ud},S'_{\rm ud}}\delta_{S_{\rm l},S'_{\rm l}}\delta_{S_{\rm r},S'_{\rm r}}\delta_{S_{\rm lr},S'_{\rm lr}}\delta_{S_{\rm env},S'_{\rm env}}\delta_{M_{\rm env},M'_{\rm env}} \\
&\quad + J_1\delta_{S_{\rm env},S'_{\rm env}}(-1)^{S_{\rm env}+S'_{\rm ud}+S_{\rm lr}}\begin{Bmatrix} S_{\rm ud} & S_{\rm lr} & S_{\rm env} \\ S'_{\rm lr} & S'_{\rm ud} & 1\end{Bmatrix}\delta_{M_{\rm env},M'_{\rm env}} \\
&\quad\times \{\langle S_{\rm l}S_{\rm r}; S_{\rm lr}\|S_{c1}\|S'_{\rm l}S'_{\rm r}; S'_{\rm lr}\rangle\langle i_{\rm up}S_{\rm up}i_{\rm down}S_{\rm down}; S_{\rm ud}\|S_{c2} \\
&\quad\times \|i'_{\rm up}S'_{\rm up}i'_{\rm down}S'_{\rm down}; S'_{\rm ud}\rangle \\
&\quad + \langle S_{\rm l}S_{\rm r}; S_{\rm lr}\|S_{d1}\|S'_{\rm l}S'_{\rm r}; S'_{\rm lr}\rangle\langle i_{\rm up}S_{\rm up}i_{\rm down}S_{\rm down}; S_{\rm ud}\|S_{d2} \\
&\quad\times \|i'_{\rm up}S'_{\rm up}i'_{\rm down}S'_{\rm down}; S'_{\rm ud}\rangle \\
&\quad + \langle S_{\rm l}S_{\rm r}; S_{\rm lr}\|S_{c5}\|S'_{\rm l}S'_{\rm r}; S'_{\rm lr}\rangle\langle i_{\rm up}S_{\rm up}i_{\rm down}S_{\rm down}; S_{\rm ud}\|S_{c4} \\
&\quad\times \|i'_{\rm up}S'_{\rm up}i'_{\rm down}S'_{\rm down}; S'_{\rm ud}\rangle \\
&\quad + \langle S_{\rm l}S_{\rm r}; S_{\rm lr}\|S_{d5}\|S'_{\rm l}S'_{\rm r}; S'_{\rm lr}\rangle\langle i_{\rm up}S_{\rm up}i_{\rm down}S_{\rm down}; S_{\rm ud}\|S_{d4} \\
&\quad\times \|i'_{\rm up}S'_{\rm up}i'_{\rm down}S'_{\rm down}; S'_{\rm ud}\rangle\}.
\end{aligned} \tag{15}$$

The terms in $\{\cdots\}$ include the product of the reduced matrix elements given by equations (A.2) and (A.3) for spins that enter into the left/right dimers and by equations (A.4) and (A.5) for the constituents of the fork-like parts.

After finding the environment eigenvalues $E_{i_{\rm env}S_{\rm env}}$ and eigenfunctions

$$|i_{\rm env}S_{\rm env}M_{\rm env}\rangle = \sum\beta^{i_{\rm env}S_{\rm env}}_{(i_{\rm up}S_{\rm up}i_{\rm down}S_{\rm down})S_{\rm ud},(S_{\rm l}S_{\rm r})S_{\rm lr}} \times |(i_{\rm up}S_{\rm up}i_{\rm down}S_{\rm down})S_{\rm ud}, (S_{\rm l}S_{\rm r})S_{\rm lr}; S_{\rm env}M_{\rm env}\rangle, \tag{16}$$

one calculates reduced matrix elements for the environment spins that directly interact with the central dimer, within the basis (see equation (A.6)).

As the final step of the diagonalization procedure one builds the basis of the entire cluster

$$|i_{\rm env}S_{\rm env}, S_c; SM\rangle = \sum_{M_{\rm env}M_c}\begin{bmatrix} S_{\rm env} & S_c & S \\ M_{\rm env} & M_c & M\end{bmatrix} \times |i_{\rm env}S_{\rm env}M_{\rm env}\rangle|S_cM_c\rangle,$$

and determines the matrix elements of the cluster Hamiltonian (7)

$$\begin{aligned}
&\langle i_{\rm env}S_{\rm env}, S_c; SM|H|i'_{\rm env}S'_{\rm env}, S'_c; S'M'\rangle = (E_{i_{\rm env}S_{\rm env}} + E_{S_c}) \\
&\quad\times \delta_{i_{\rm env},i'_{\rm env}}\delta_{S_{\rm env},S'_{\rm env}}\delta_{S_c,S'_c}\delta_{S,S'}\delta_{M,M'} \\
&\quad + J_1(-1)^{S+S'_{\rm env}+S_c}\begin{Bmatrix} S_{\rm env} & S_c & S \\ S'_c & S'_{\rm env} & 1\end{Bmatrix}\delta_{S,S'}\delta_{M,M'}
\end{aligned}$$

$$\times \left[\langle S_c \| S(1) \| S_c' \rangle \sum_{k=c2,c4} \langle i_{\rm env} S_{\rm env} \| S_k \| i'_{\rm env} S'_{\rm env} \rangle \right.$$

$$\left. + \langle S_c \| S(2) \| S_c' \rangle \sum_{k=d2,d4} \langle i_{\rm env} S_{\rm env} \| S_k \| i'_{\rm env} S'_{\rm env} \rangle \right], \qquad (17)$$

where RMEs are previously derived (see equations (9), (10) and (A.6)). Numerical diagonalization of the matrix (17) yields the target spectrum E_{iS} and eigenfunctions

$$|iSM\rangle = \sum \gamma^{iS}_{S_{\rm env} M_{\rm env}, S_c} |S_{\rm env} M_{\rm env}, S_c; SM\rangle. \qquad (18)$$

3. The truncation procedure

The classification of eigenstates of the parts we used to gather the total cluster according to irreducible representations of the $SU(2)$-group enables us to organize the truncation procedure inside sectors of Hilbert space that arise at consecutive steps of the algorithm. A possibility to carry out calculations within a reduced basis is a feature of the algorithm that relates it with other renormalization group methods.

We hold the following strategy of the truncation procedure to build target states that are obtained after combining two parts of the lattice. For a given spin-S sector a certain amount of states having the lowest energies are kept. Thus each group of $|iS\rangle$ states is presented in a reduced basis. We truncate the basis of two 'fork'-like parts before combining them into a larger lattice segment. This is not the only way to do so, for example one can truncate the basis of the environment after combining the 'fork'-like parts, but the former is easier to perform.

We tested several realizations of the truncation procedure, either by simply controlling a number of vectors retained in the reduced basis, or by monitoring a genealogy of the target spin-S state through the triangle rule, i.e. only states that contribute to the target state are taken into account. The last approach gives an opportunity to keep more vectors in the basis due to omitting of redundant states. Moreover, the highest-spin cluster states, i.e. those with $S \geqslant 15$ in our problem, are treated exactly. The size of the truncated basis was chosen equal to either 64 or 121 for the scheme without taking genealogy of the target state into account, and it varies from 12 up to 352, being dependent on the total spin S, for the 'genealogical' scheme.

The accuracy of the truncation procedure is controlled by monitoring the energy of the lowest state within each spin sector. The variation of this observable, computed through both the schemes, does not normally exceed 1–2% (a maximum discrepancy of the order 6% is reached only in the S-8 sector); this provides evidence for the correctness of the constructed basis, which exhibits almost no dependence on the used truncation procedure. The results that we present below are obtained within the 'genealogical' scheme.

Another feature of the algorithm is combining the central unit (one site or dimer) with its environment at the final step. The procedure does not depend on the structure of the environment and looks similar for any cluster. However, the information about quantum numbers of the environment states enables us to simplify the calculations substantially at this stage of the algorithm. Indeed, for a given spin-S sector of the Hilbert space of the entire cluster, one should pick out only those environment eigenfunctions for which the spins S_u obey the rule

$$|S_u - S_c| \leqslant S \leqslant S_u + S_c.$$

Using the truncation procedure results in bases composed from a maximum of 4–5 thousand states. To control the accuracy of the procedure, results obtained for the 18-site system are compared with those for the 10-site system. The smaller cluster enables us to handle the complete basis without any truncation. The 10-site system is embedded into a bigger cluster and consists of the following parts: the central dimer $c3, d3$ and neighbor dimers $b2, c2, b4, c4, d2, e2$ and $d4, e4$. Apparently, the construction of the environment requires two consecutive steps (i) addition of dimers $b2, c2$ and $b4, c4$ as well as $d2, e2$ and $d4, e4$ ones according to equation (12), followed by calculation of the reduced matrix elements according to equation ((A.2) and (A.3)); (ii) construction of the environment states from the upper and lower parts built previously and the calculation of the RME of the environment spins that interact directly with the central dimer. The entire cluster Hamiltonian is obtained through (17). The biggest Hilbert space dimension (2025 × 2025) is reached in the S-2 sector. Numerical results for the supplementary cluster are listed in table 1 for comparison. Note that one should compare energy values with the same magnetization per dimer (see figure 2).

Table 1. Numerical results of the lowest energy $E_{\rm min}$ and the energy $\tilde{\varepsilon}$ per dimer in the spin-S subspaces for $N = 10$ and 18 clusters.

S	$E_{\rm min}$ $(N = 10)/J_0$	$\tilde{\varepsilon}$ $(N = 10)$	$E_{\rm min}$ $(N = 18)/J_0$	$\tilde{\varepsilon}$ $(N = 18)$
0	−10.0334	−2.0067	−18.0336	−2.0037
1	−9.1853	−1.8371	−17.1431	−1.9048
2	−8.2123	−1.6425	−16.2529	−1.8059
3	−7.1978	−1.4396	−15.2935	−1.6993
4	−6.1430	−1.2286	−14.3205	−1.5912
5	−4.9344	−0.9869	−13.3164	−1.4796
6	−2.9787	−0.5957	−12.2745	−1.3638
7	−0.9610	−0.1922	−11.1879	−1.2431
8	1.0849	0.2170	−10.0260	−1.1140
9	3.1588	0.6318	−8.8335	−0.9815
10	5.4418	1.0883	−6.8807	−0.7645
11			−4.8994	−0.5444
12			−2.8795	−0.3199
13			−0.8172	−0.0908
14			1.2815	0.1424
15			3.4533	0.3837
16			5.6844	0.6316
17			7.960	0.8844
18			10.3254	1.1473

4. The energy spectrum and magnetization curve

The results of the energy spectrum calculation for two $N = 10$ and 18 clusters are listed in table 1, where the minimal energy $E_{\rm min}$ within each spin-S sector along with energy per dimer $\tilde{\varepsilon} = 2E_{\rm min}/N$ are given. The magnetization per dimer is determined by $m = 2S/N$. Both $N = 10$ and 18 dependences $\tilde{\varepsilon}(m)$ are shown together in figure 2. Points for both clusters lay on the same curve, i.e. finite-size effects can be ignored, which

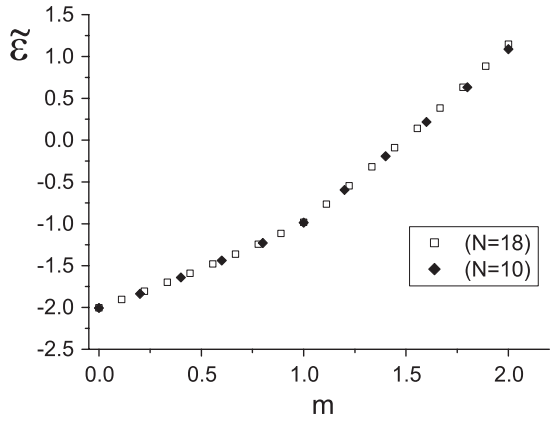

Figure 2. Plot of the lowest energy per dimer $\tilde{\varepsilon}\ (m)$ versus m for the $N = 10$ and 18 clusters. The cusp is seen at $m = 1$.

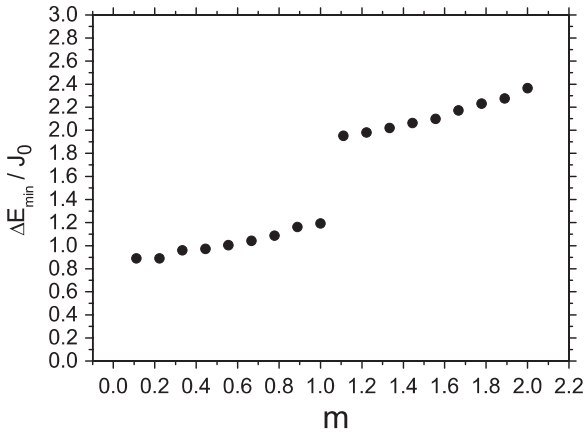

Figure 3. Plot of the changes $\Delta E_{\min}$ versus the dimer magnetization m. A distinct jump is seen at $m = 1$.

is expected for the regime of a small dimer–dimer interaction $J_1 \ll J_0$.

A remarkable feature of the curve is the cusp in the middle, i.e. at $m = 1$. Independent fitting of both parts by the quadratic form $\varepsilon(m) = \varepsilon_2 m^2 + \varepsilon_1 m + \varepsilon_0$ jointed in the point yields $\varepsilon_2 = 0.190 \pm 0.018$, $\varepsilon_1 = 0.828 \pm 0.019$, and $\varepsilon_0 = -2.0073 \pm 0.0040$ for lower part of the curve ($0 < m < 1$) together with $\varepsilon_2 = 0.200 \pm 0.058$, $\varepsilon_1 = 1.4578 \pm 0.018$, and $\varepsilon_0 = -2.629 \pm 0.014$ for upper part ($1 < m < 2$).

Based on $N = 18$ case data we build a dependence of jumps $E_{\min}$ when the total spin S changes from 0 up to 18, or the dimer magnetization varies from 0 up to 2 (figure 3). One can see that the values of jumps are approximately J_0 for $S \leqslant 9$ and they increase by a factor of 2 as $S \geqslant 10$. It means that the energy of the total system of weakly interacting dimers changes with an increase of magnetic field, due to local excitations inside separate dimers. Indeed, for the single $S = 1$ dimer the spectrum consists of a singlet, a triplet, and a quintuplet. The energy difference between the singlet and the triplet is J_0, while the difference between the quintuplet and the triplet is $2J_0$ (see the discussion in section 5).

A standard way to describe the magnetization process at $T = 0$ is to define $E^{(S)}_{\min}(N)$ as the lowest energy of the

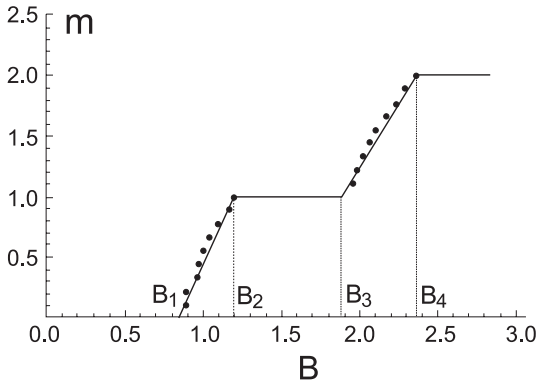

Figure 4. Plot of m versus B obtained via $B = \varepsilon'(m)$. The dots mark values found through the diagonalization algorithm.

Hamiltonian (1) in the spin-S subspace for the finite system of N elementary dimers. Applying a magnetic field B leads to the Zeeman splitting of the energy levels $E^{(S)}_{\min}(B) = E^{(S)}_{\min} - SB$, and therefore, the level crossing occurs at values $B_S = E^{(S+1)}_{\min}(B) - E^{(S)}_{\min}(B)$ when the field is increased. These level crossings correspond to jumps of value $1/N$ in magnetization at zero temperature, until the fully polarized state with magnetization per dimer $m_{\text{sat}} = 2N/N = 2$ is reached at a value of the magnetic field $B_{\text{sat}} = E^{(2N)}_{\min}(B) - E^{(2N-1)}_{\min}(B)$. The calculation performed for $N/2 = 9$ dimers yields the magnetization points presented in figure 4 and reveals the appearance of the ground state plateau as well as the plateau at one-half of the saturation value.

To guarantee the validity of the magnetization curve we use the approach developed by Sakai and Takahashi [17] to recover the $m(B)$ dependence in the thermodynamic limit. In this case the condition for crossover fields transforms into $B = \varepsilon'(m)$, where ε is the energy per dimer. The plateau boundaries are determined by the derivatives at the special points: (i) $B_1 = \varepsilon'(+0)$ is related with the end of the ground state plateau; (ii) $B_2 = \varepsilon'(1-0)$ and $B_3 = \varepsilon'(1+0)$ correspond to the beginning and the end of intermediate plateau, respectively; (iii) $B_4 = \varepsilon'(2-0)$ marks an emergence of saturation magnetization.

Treating the energy spectrum results in linear dependences relevant to the sectors between plateaus

$$\begin{cases} \varepsilon'(m) = 0.83 + 0.38m, & 0 < m < 1, \\ \varepsilon'(m) = 1.46 + 0.40m, & 1 < m < 2, \end{cases} \tag{19}$$

that yields immediately $B_1 = 0.83J_0$, $B_2 = 1.21J_0$, $B_3 = 1.86J_0$, and $B_4 = 2.26J_0$. Values normalized to the saturation field B_{sat} are listed in table 2 and exhibit a reasonable agreement with the experimental data for the F_2PNNNO system. A comparison of finite cluster calculations with those of the thermodynamic limit (19) is given in figure 4. One can see that both methods come to close results.

Note that the method we used for numerical calculations is intrinsically a two-dimensional one, whereas the previous numerical study of the system [12] dealt with an essentially one-dimensional 'folded chain' cluster. The regions between the plateaus of the magnetization curve exhibit a behavior closer to a linear one instead of the S-shape forms obtained earlier.

Table 2. Values of the magnetic field special points compared with the experimental data.

$B_i/B_{\rm sat}$	$i=1$	$i=2$	$i=3$	$i=4$
Theory	0.37	0.53	0.82	1
Experiment [12]	0.33	0.53	0.89	1

5. The semi-hard-core boson model

Here we introduce the boson picture based on data presented in figure 3. For $J_1 \ll J_0$ the low energy subspace of the spin Hamiltonian (1) consists of the singlet, the $S^z = 1$ component of the triplet, and the $S^z = 2$ component of the quintuplet. It is convenient to identify the triplet state with the presence of a bosonic particle (triplon), the quintuplet state as a pair of bosons (quintuplon), and the singlet state as an absence of bosons. Then, the boson model is formulated via the semi-hard-core bosonic operators g_i and $g_i^\dagger$ with the extended Pauli exclusion principle $g_i^{\dagger 3} = 0$, i.e. more than two bosons per site are forbidden. Note that this principle may be realized via parafermion language, but its description requires a transmutation of statistics that complicates calculations in a 2D case (see appendix B). The algebra of the operators is $[g_i, g_i] = [g_i^\dagger, g_i^\dagger] = 0$, and $[g_i, g_i^\dagger] = \delta_{ij}(1 - F_i)$, where $F_i = (3/2)n_i(n_i - 1)$ is deformation of the canonical boson algebra, $n_i = g_i^\dagger g_i$ is the number operator [10].

The boson Hamiltonian in terms of these operators is written as

$$H = \tfrac{1}{2}\sum_{\langle ij\rangle}(g_i^\dagger g_j + g_j^\dagger g_i)(h_1 + h_2 + h_3) - \mu\sum_i n_i + \frac{U}{2}\sum_i n_i(n_i+1) + V\sum_{\langle ij\rangle}(n_i - 1)(n_j - 1), \qquad (20)$$

where the hopping terms

$$h_1 = t_1(n_{ij} - 2)(n_{ij} - 3), \qquad h_2 = 2t_2(n_{ij} - 1)(3 - n_{ij}),$$

$$h_1 = t_3(n_{ij} - 1)(n_{ij} - 2)$$

depend on the number of particles $n_{ij} = n_i + n_j$ on the bonds i, j.

The map between the bosonic (20) and the spin Hamiltonian (1) is reached through representation [11] (see figure 5)

$$n_i = S_i^z = S_{i1}^z + S_{i2}^z,$$

where (1, 2) marks two spins on each dimer, and

$$g_i^\dagger = \frac{1}{\sqrt{2}}(S_{i2}^\dagger - S_{i1}^\dagger)\left[\frac{\sqrt{3}}{2\sqrt{2}} + \left(1 - \frac{\sqrt{3}}{2\sqrt{2}}\right)S_i^z\right].$$

This establishes the relationship between the spin and the bosonic parameters $U = J_0$, $V = J_1/2$, $\mu = B - 4J_1$, and $t_i = -\frac{8\sqrt{2}}{3\sqrt{3}}a^i J_1$, where $a = \frac{\sqrt{3}}{2\sqrt{2}}(i = 1, 2, 3)$. Thus, the bosonic model includes a strong on-site boson repulsion U as well as a noticeable repulsive inter-site interaction V. The magnetic field B plays the role of the chemical potential μ.

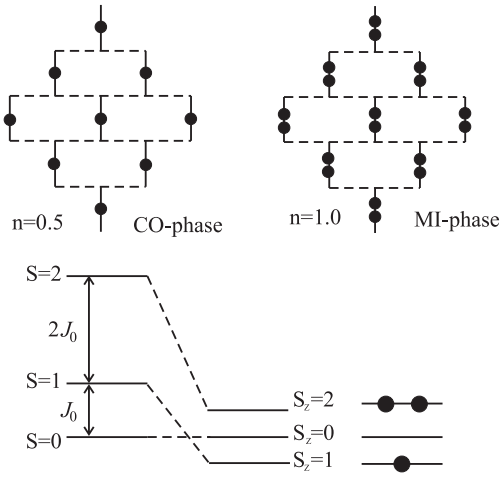

Figure 5. The low energy subspace of the single dimer spectrum in the presence of a magnetic field. Boson superlattice patterns corresponding to the charge-ordered and Mott insulating phases are shown above.

The boson Hamiltonian (20) constitutes a low energy effective model of the spin Hamiltonian (1) that emerges from restricting H_S to the subspace of the semi-hard-core bosonic operators. The map is valid in the limit $J_1 \ll J_0$, or in the boson language t_i/U, $V/U \ll 1$, when the main physics is governed by a competition between one-site repulsion and chemical potential.

The quantum phase diagram of the boson Hamiltonian (20) was built in [11] by using the stochastic series expansion quantum Monte Carlo method (see their figure 4). It has been found that a Bose condensate fraction appears in the regions of the chemical potential (magnetic field) between the plateaus of the g-particles density (magnetization curve). In contrast, the charge density wave (Ising-like charge order (CO) phase) forms around the intermediate plateau. There are regions, where a supersolid phase, a mixing of the charge order and the Bose-superfluid (BS), emerges. According to this study, the magnetization curve shown in figure 4 can be interpreted as tuning of boson density by an applied magnetic field. At a small chemical potential, the lowest energy is achieved by empty states, i.e. those where all dimers are in the singlet state (boson vacuum). For $B > B_1$ a finite density of bosons (triplons) emerges in the ground state and contributes to the BS phase. The triplon excitations are mobile due to weak inter-dimer coupling. The density (magnetization) increases monotonically as a function of magnetic field until B_2, where a transition to the CO-phase occurs. This corresponds to the boson concentration $n = 0.5$, when the triplons crystallize in a superstructure pattern (figure 5). The fractional plateau requires strong boson interactions in comparison to the kinetic energy. At $B > B_3$ the filling increases monotonically in the resulting BS phase (quintuplon condensation) until the ground state transforms into a Mott insulating (MI) phase with two bosons per dimer at $B > B_4$. The boson concentration in the MI phase is $n = 1$. The reasonings are easily reproduced if one analyzes the boson Hamiltonian (20) by neglecting the inter-site terms.

6. Conclusions

Quantum dimer antiferromagnetic systems are a good field for studying the BEC of interacting particles. Along with ultracold atomic gases in optical lattices [18, 19] they offer an opportunity to observe transitions predicted by lattice boson models. In many cases, the boson picture is more transparent physically than the original spin language. Based on the analysis of the finite cluster energy spectrum for the two-dimensional spin-1 organic antiferromagnet F_2PNNNO with dimerized structure, we prove the relevance of semi-hard-core bosons with pronounced on-site and inter-site repulsions for a low-dimensional spin system. The unusual magnetization curve observed in F_2PNNNO is nothing but a manifestation of the fine tuning of the density of bosons by an applied magnetic field, when a low-density Bose-superfluid, charge ordering with one boson per dimer, and a high-density Bose-superfluid phases change each other subsequently with field increases.

Acknowledgments

We would like to thank T Sakai, J Kishine and N V Baranov for discussions. VES would like to acknowledge the support of the US Civilian Research & Development Foundation (CRDF) and the Ministry of Education and Science of the Russian Federation (MinES) under the 'Basic Research and Higher Education' (BRHE) program.

Appendix A

The reduced matrix elements for spins on $c2$ and $c4$ sites computed in the basis of eigenfunctions of the Hamiltonian $H_{\rm down}$ are given by the 141 × 141 matrix

$$\begin{aligned}&\langle i_{\rm down}S_{\rm down}\|S_{c2(c4)}\|i'_{\rm down}S'_{\rm down}\rangle\\&=\sum_{S_2S_3S_4S_{24}}\sum_{S'_2S'_3S'_4S'_{24}}\alpha^{i_{\rm down}S_{\rm down}}_{(S_2S_4)S_{24},S_3}\alpha^{i'_{\rm down}S'_{\rm down}}_{(S'_2S'_4)S'_{24},S'_3}\\&\quad\times\langle(S_2S_4)S_{24},S_3;S_{\rm down}\|S_{c2(c4)}\|(S'_2S'_4)S'_{24},S'_3;S'_{\rm down}\rangle.\end{aligned}\tag{A.1}$$

The reduced matrix elements that enter into the expression are calculated according to the rules

$$\begin{aligned}&\langle(S_2S_4)S_{24},S_3;S_{\rm down}\|S_{c2}\|(S'_2S'_4)S'_{24},S'_3;S'_{\rm down}\rangle\\&=(-1)^{S_2+S_4+S_3+S_{24}+S'_{24}+S'_{\rm down}}[S_{24},S'_{24},S_{\rm down},S'_{\rm down}]^{1/2}\\&\quad\times\begin{Bmatrix}S_{24}&1&S'_{24}\\S'_2&S_4&S_2\end{Bmatrix}\begin{Bmatrix}S_{\rm down}&1&S'_{\rm down}\\S'_{24}&S_3&S_{24}\end{Bmatrix}\\&\quad\times\langle11;S_2\|S(2)\|11;S'_2\rangle\delta_{S_4S'_4}\delta_{S_3S'_3},\\&\langle(S_2S_4)S_{24},S_3;S_{\rm down}\|S_{c4}\|(S'_2S'_4)S'_{24},S'_3;S'_{\rm down}\rangle\\&=(-1)^{S_2+S'_4+S_3+2S_{24}+S'_{\rm down}}[S_{24},S'_{24},S_{\rm down},S'_{\rm down}]^{1/2}\\&\quad\times\begin{Bmatrix}S_{24}&1&S'_{24}\\S'_4&S_2&S_4\end{Bmatrix}\begin{Bmatrix}S_{\rm down}&1&S'_{\rm down}\\S'_{24}&S_3&S_{24}\end{Bmatrix}\\&\quad\times\langle11;S_4\|S(2)\|11;S'_4\rangle\delta_{S_2S'_2}\delta_{S_3S'_3},\end{aligned}$$

where $[S]=(2S+1)$.

The reduced matrix elements for spins on the sites $c1$ ($d1$) are given by the 19 × 19 matrix built in the basis of functions, which are constructed from the 'left' and the 'right' dimers equation (12)

$$\begin{aligned}&\langle S_{\rm l}S_{\rm r};S_{\rm lr}\|S_{c1(d1)}\|S'_{\rm l}S'_{\rm r};S'_{\rm lr}\rangle\\&=\sqrt{(2S_{\rm lr}+1)(2S'_{\rm lr}+1)}(-1)^{1+S_{\rm l}+S_{\rm r}+S'_{\rm lr}}\\&\quad\times\begin{Bmatrix}S_{\rm lr}&1&S'_{\rm lr}\\S'_{\rm l}&S_{\rm r}&S_{\rm l}\end{Bmatrix}\langle11;S_{\rm l}\|S(1(2))\|11;S'_{\rm l}\rangle\delta_{S_{\rm r}S'_{\rm r}}.\end{aligned}\tag{A.2}$$

The RME for spins on the $c5$ ($d5$) sites are calculated as follows:

$$\begin{aligned}&\langle S_{\rm l}S_{\rm r};S_{\rm lr}\|S_{c5(d5)}\|S'_{\rm l}S'_{\rm r};S'_{\rm lr}\rangle\\&=\sqrt{(2S_{\rm lr}+1)(2S'_{\rm lr}+1)}(-1)^{1+S_{\rm l}+S'_{\rm r}+S_{\rm lr}}\\&\quad\times\begin{Bmatrix}S_{\rm lr}&1&S'_{\rm lr}\\S'_{\rm r}&S_{\rm l}&S_{\rm r}\end{Bmatrix}\langle11;S_{\rm r}\|S(1(2))\|11;S'_{\rm r}\rangle\delta_{S_{\rm l}S'_{\rm l}}.\end{aligned}\tag{A.3}$$

The reduced matrix elements of spin operators on sites $c2(d2)$, $c4(d4)$ calculated on the eigenfunctions of the up and down parts form the 73 789 × 73 789 matrices.

$$\begin{aligned}&\langle i_{\rm up}S_{\rm up}i_{\rm down}S_{\rm down};S_{\rm ud}\|S_{c2(c4)}\|i'_{\rm up}S'_{\rm up}i'_{\rm down}S'_{\rm down};S'_{\rm ud}\rangle\\&=\sqrt{(2S_{\rm ud}+1)(2S'_{\rm ud}+1)}(-1)^{1+S_{\rm up}+S'_{\rm down}+S_{\rm ud}}\\&\quad\times\begin{Bmatrix}S_{\rm ud}&1&S'_{\rm ud}\\S'_{\rm down}&S_{\rm up}&S_{\rm down}\end{Bmatrix}\langle i_{\rm down}S_{\rm down}\|S_{c2(c4)}\\&\quad\times\|i'_{\rm down}S'_{\rm down}\rangle\delta_{i_{\rm up}i'_{\rm up}}\delta_{S_{\rm up}S'_{\rm up}}.\end{aligned}\tag{A.4}$$

$$\begin{aligned}&\langle i_{\rm up}S_{\rm up}i_{\rm down}S_{\rm down};S_{\rm ud}\|S_{d2(d4)}\|i'_{\rm up}S'_{\rm up}i'_{\rm down}S'_{\rm down};S'_{\rm ud}\rangle\\&=\sqrt{(2S_{\rm ud}+1)(2S'_{\rm ud}+1)}(-1)^{1+S_{\rm up}+S_{\rm down}+S'_{\rm ud}}\\&\quad\times\begin{Bmatrix}S_{\rm ud}&1&S'_{\rm ud}\\S'_{\rm up}&S_{\rm down}&S_{\rm up}\end{Bmatrix}\langle i_{\rm up}S_{\rm up}\|S_{d2(d4)}\\&\quad\times\|i'_{\rm up}S'_{\rm up}\rangle\delta_{i_{\rm down}i'_{\rm down}}\delta_{S_{\rm down}S'_{\rm down}}.\end{aligned}\tag{A.5}$$

The reduced matrix elements of the spin operators on sites $c2(d2)$, $c4(d4)$ are calculated on eigenfunctions of the environment. The dimension of these matrices is determined by the dimension of the truncated basis of the environment

$$\begin{aligned}&\langle i_{\rm env}S_{\rm env}\|S_k\|i'_{\rm env}S'_{\rm env}\rangle=\sum\beta^{i_{\rm env}S_{\rm env}}_{(i_{\rm up}S_{\rm up}i_{\rm down}S_{\rm down})S_{\rm ud},(S_{\rm l}S_{\rm r})S_{\rm lr}}\\&\quad\times\beta^{i'_{\rm env}S'_{\rm env}}_{(i'_{\rm up}S'_{\rm up}i'_{\rm down}S'_{\rm down})S'_{\rm ud},(S'_{\rm l}S'_{\rm r})S'_{\rm lr}}\\&\quad\times\langle(i_{\rm up}S_{\rm up}i_{\rm down}S_{\rm down})S_{\rm ud},(S_{\rm l}S_{\rm r})S_{\rm lr};S_{\rm env}\|S_k\\&\quad\times\|(i'_{\rm up}S'_{\rm up}i'_{\rm down}S'_{\rm down})S'_{\rm ud},(S'_{\rm l}S'_{\rm r})S'_{\rm lr};S'_{\rm env}\rangle,\end{aligned}\tag{A.6}$$

where $k=c2(d2)$, $c4(d4)$ and

$$\begin{aligned}&\langle(i_{\rm up}S_{\rm up}i_{\rm down}S_{\rm down})S_{\rm ud},(S_{\rm l}S_{\rm r})S_{\rm lr};S_{\rm env}\|S_k\\&\quad\times\|(i'_{\rm up}S'_{\rm up}i'_{\rm down}S'_{\rm down})S'_{\rm ud},(S'_{\rm l}S'_{\rm r})S'_{\rm lr};S'_{\rm env}\rangle\\&=\sqrt{(2S_{\rm env}+1)(2S'_{\rm env}+1)}\\&\quad\times(-1)^{1+S_{\rm ud}+S_{\rm lr}+S'_{\rm env}}\begin{Bmatrix}S_{\rm env}&1&S'_{\rm env}\\S'_{\rm ud}&S_{\rm lr}&S_{\rm ud}\end{Bmatrix}\\&\quad\times\langle i_{\rm up}S_{\rm up}i_{\rm down}S_{\rm down};S_{\rm ud}\|S_k\|i'_{\rm up}S'_{\rm up}i'_{\rm down}S'_{\rm down};S'_{\rm ud}\rangle\\&\quad\times\delta_{S_{\rm l}S'_{\rm l}}\delta_{S_{\rm r}S'_{\rm r}}\delta_{S_{\rm lr}S'_{\rm lr}}.\end{aligned}\tag{A.7}$$

Appendix B

Quantum statistics is based on two principles. The first one is exchange statistics, when a permutation of two identical

particles causes an appearance of a phase factor in the total wave function. The second one is exclusion statistics, which reflects an ability to accommodate p particles in the same single-particle quantum state. Whereas the first concept depends on the space dimensionality of the system, the second one does not [20].

The exclusion statistics algebra obeying the generalized Pauli exclusion principle can be formulated in terms of the bond g operators that have been used in the main text. Another variant of the exclusion statistics can be realized, for example, via Green's parafermion statistics [21, 22]. According to common formalism based on Burnside's theorem of group theory (see [10] for details), both algebraic approaches are related to each other.

Indeed, let us introduce two modes ($\alpha = 1, 2$) for each ith bond

$$\{d_i^\alpha, d_j^\alpha\} = \{(d_i^\alpha)^\dagger, (d_j^\alpha)^\dagger\} = 0, \qquad \{d_i^\alpha, (d_j^\alpha)^\dagger\} = \delta_{ij} \tag{B.1}$$

with the condition $d_j^\alpha|\text{vacuum}\rangle = 0$. For $\alpha \neq \beta$ the modes satisfy non-standard relations

$$[d_i^\alpha, d_j^\beta] = [(d_i^\alpha)^\dagger, (d_j^\beta)^\dagger] = 0, \qquad [d_i^\alpha, (d_j^\beta)^\dagger] = 0. \tag{B.2}$$

Parafermion creation and annihilation operators are determined as

$$d_j^\dagger = (d_j^1)^\dagger + (d_j^2)^\dagger, \qquad d_j = d_j^1 + d_j^2. \tag{B.3}$$

They satisfy commutation relations

$$[[d_i^\dagger, d_j], d_l] = -2\delta_{il} d_j, \qquad [[d_i, d_j], d_l] = 0. \tag{B.4}$$

The parafermion number operator $n_j^d = (d_j^1)^\dagger d_j^1 + (d_j^2)^\dagger d_j^2$ can be written as

$$n_j^d = \tfrac{1}{2}([d_i^\dagger, d_j] + 2), \tag{B.5}$$

and obeys the commutation rule

$$[n_j^d, d_j^\dagger] = \delta_{ij} d_j^\dagger. \tag{B.6}$$

From the property $(n_j^\alpha)^2 = n_j^\alpha$ one can conclude that n_j^d varies from 0 to 2. Moreover,

$$(d_j^\dagger)^2 = 2(d_i^1)^\dagger (d_i^2)^\dagger, \tag{B.7}$$

that means $(d_j^\dagger)^3 = 0$. Therefore, the parafermion representation provides the extended Pauli exclusion principle.

To establish a connection between the bond g-algebra and the parafermion statistics, we note that the local Hilbert space related with a bond has the dimension $D = 3$. Therefore, one can map the g-particles onto the algebra of S-1 operators

$$S_i^+ = \sqrt{2} g_i^\dagger \left[1 + \left(\frac{1}{\sqrt{2}} - 1\right) n_i^g\right],$$
$$S_i^- = \sqrt{2}\left[1 + \left(\frac{1}{\sqrt{2}} - 1\right) n_i^g\right] g_i, \qquad S_i^z = n_i^g - 1. \tag{B.8}$$

These spin operators are connected with two-flavor hard-core bosons via the generalization of the Jordan–Wigner transformation [23, 24]

$$S_i^+ = \sqrt{2}(b_{i1}^\dagger + b_{i2}), \qquad S_i^- = \sqrt{2}(b_{i1} + b_{i2}^\dagger),$$
$$S_i^z = b_{i1}^\dagger b_{i1} - b_{i2}^\dagger b_{i2} \tag{B.9}$$

with the imposed constraint $b_{i1}^\dagger b_{i1} + b_{i2}^\dagger b_{i2} = 1$, and the spin state $S^z = 0$ is taken as a vacuum. The commutation relations for the hard bosons are

$$[b_{i\alpha}, b_{i\beta}] = [b_{i\alpha}^\dagger, b_{i\beta}^\dagger] = 0,$$
$$[b_{i\alpha}, b_{i\beta}^\dagger] = \delta_{ij}\delta_{\alpha\beta}(1 - n_{i\alpha}^b), \qquad [n_{i\alpha}^b, b_{j\beta}^\dagger] = \delta_{ij}\delta_{\alpha\beta} b_{i\alpha}^\dagger, \tag{B.10}$$

where $n_{i\alpha}^b = b_{i\alpha}^\dagger b_{i\alpha}$ ($\alpha = 1, 2$) is the number operator for the hard bosons.

A transition from the hard-core bosons to the parafermions is related with a transmutation of statistics. In the two-dimensional case, the change of statistics is based on a generalization of the conventional Jordan–Wigner transformation [25, 26]. In the following, for simplicity, we will illustrate the connection on an example of dimerized one-dimensional S-1 chain.

The parafermion modes are converted into the canonical two-flavor canonical fermions $c_{i\alpha}$ ($\alpha = 1, 2$) determined on the ith bond of the chain through the *partial* non-local transmutators

$$(d_i^1)^\dagger = c_{i1}^\dagger \exp\left[\mathrm{i}\pi \sum_{j<i} n_{j2}\right],$$
$$(d_i^2)^\dagger = c_{i2}^\dagger \exp\left[\mathrm{i}\pi\left(\sum_{j<i} n_{j1} + n_{i1}\right)\right], \tag{B.11}$$

where

$$\{c_{i\alpha}, c_{j\beta}\} = \{c_{i\alpha}^\dagger, c_{j\beta}^\dagger\} = 0, \qquad \{c_{i\alpha}, c_{j\beta}^\dagger\} = \delta_{ij}\delta_{\alpha\beta}, \tag{B.12}$$

and $n_{i\alpha} = c_{i\alpha}^\dagger c_{i\alpha}$ is the number operator for the fermions.

A map between the hard-core bosons and the two-flavor fermions is established by the *total* non-local transmutators

$$b_{i1}^\dagger = c_{i1}^\dagger \exp\left[\mathrm{i}\pi \sum_{j<i}(c_{j1}^\dagger c_{j1} + c_{j2}^\dagger c_{j2})\right],$$
$$b_{i2}^\dagger = c_{i2}^\dagger \exp\left[\mathrm{i}\pi \sum_{j<i}(c_{j1}^\dagger c_{j1} + c_{j2}^\dagger c_{j2})\right] \mathrm{e}^{\mathrm{i}\pi c_{j1}^\dagger c_{j1}}. \tag{B.13}$$

Relations (B.8), (B.9), (B.11), (B.13) provide the mapping between the parafermions and the g-particles.

References

[1] Affleck I 1990 *Phys. Rev.* B **41** 6697
Giamarchi T and Tsvelik A M 1999 *Phys. Rev.* B **59** 11398
[2] Giamarchi T, Rüegg C and Tchernyshyov O 2008 *Nat. Phys.* **4** 198
[3] Rice T M 2002 *Science* **298** 760
[4] Nikuni T *et al* 2008 *Phys. Rev. Lett.* **84** 5868

[5] Rüegg C *et al* 2003 *Nature* **423** 62
[6] Sebastian S E *et al* 2006 *Nature* **441** 617
[7] Kofu M, Kim J-H, Ji S, Lu S-H, Ueda H, Qin Y, Kang H-J, Green M A and Ueda Y 2009 *Phys. Rev. Lett.* **102** 037206
[8] Tsuji H, Andraka B, Ushida M, Tanaka H and Takano Y 2005 *Phys. Rev.* B **72** 214434
[9] Stone M B, Lumsden M D, Chang S, Samulon E C, Batista C D and Fisher I R 2008 *Phys. Rev. Lett.* **100** 237201
[10] Batista C D and Ortiz G 2004 *Adv. Phys.* **53** 1
[11] Sengupta P and Batista C D 2007 *Phys. Rev. Lett.* **98** 227201
[12] Hosokoshi Y, Nakazawa Y, Inoue K, Takizawa K, Nakano H, Takahashi M and Goto T 1999 *Phys. Rev.* B **60** 12924
[13] Tsujii H, Andraka B, Hosokoshi Y, Inoue K and Takano Y 2007 *J. Magn. Magn. Mater.* **310** 415
[14] Boyarchenkov A S, Bostrem I G and Ovchinnikov A S 2007 *Phys. Rev.* B **76** 123456
[15] Sinitsyn V E, Bostrem I G and Ovchinnikov A S 2007 *J. Phys. A: Math. Theor.* **40** 645
[16] Sato M 2005 *Phys. Rev.* B **71** 024402
[17] Sakai T and Takahashi M 1991 *Phys. Rev.* B **43** 13383
Sakai T and Takahashi M 1998 *Phys. Rev.* B **57** R3201
[18] Grenier M, Mandel O, Esslinger T, Hänsch T W and Bloch I 2002 *Nature* **415** 39
[19] Bloch I 2005 *Nat. Phys.* **1** 23
[20] Haldane F D M 1991 *Phys. Rev. Lett.* **67** 937
[21] Green H S 1953 *Phys. Rev.* **90** 270
[22] Green H S 1972 *Prog. Theor. Phys.* **47** 1400
[23] Batista C D and Ortiz G 2001 *Phys. Rev. Lett.* **86** 1082
[24] Sengupta P and Batista C D 2007 *Phys. Rev. Lett.* **99** 217205
[25] Fradkin E 1989 *Phys. Rev. Lett.* **63** 322
[26] Wang Y R 1991 *Phys. Rev.* B **43** 3786